

# Chapter 1

## The COMPASS Experiment at CERN

The COmmon Muon Proton Apparatus for Structure and Spectroscopy (COMPASS) experiment is a fixed target experiment located in France in the North Area at CERN. COMPASS started taking data in 2002 in the same hall as earlier European Muon Collaboration (EMC), New Muon Collaboration (NMC) and Spin Muon Collaboration (SMC) experiments. COMPASS has studied hadron structure through (SI)DIS, Drell-Yan and Primakoff reactions and has done hadron spectroscopy measurements.

CERN is the European Organization for Nuclear physics research. It is located part in France and part in Switzerland and includes many experiments and accelerators providing beam to these experiments. The accelerator beam lines are connected and feed beam to each other resulting in an increase in beam momentum at each successive accelerator. A schematic of the accelerators at CERN is shown in Fig. 1.1 where the accelerator that sends beam to COMPASS is the Super Proton Synchrotron (SPS).

The COMPASS spectrometer is a two-stage spectrometer. The two stages are series where each stage contains various tracking detectors and a muon wall filter at the end of each stage. Any particles that penetrate through the active area of either of the muon wall filters are with a high probability, muons. Both stages also contain an electromagnetic and hadron calorimeter. The stages are both centered around a strong spectrometer magnet used for determining particle momentum. The first stage downstream of the target is the large angle spectrometer (LAS) and it is centered around the SM1 magnet which has an integrated field of 1 Tm. This stage detects tracks with larger polar scattering angles roughly between 26 mrad and 160 mrad. The second stage is the small angle spectrometer (SAS) and it detects particle tracks having a scattering angle between roughly 8 mrad and 45 mrad. This stage is centered around the SM2 magnetic which has an integrated field of 4.4 Tm.

The left and right side of the spectrometer are referred to by the mountains that surround the spectrometer. When looking down the beam line the left side is referred to as the Jura side which roughly corresponds to the west side and the right side is referred to as the Saleve side which roughly corresponds to the east side. A graphic of the 2015 setup is shown in Fig 1.2.

This chapter gives an overview of the general COMPASS data taking setup and highlights the specific

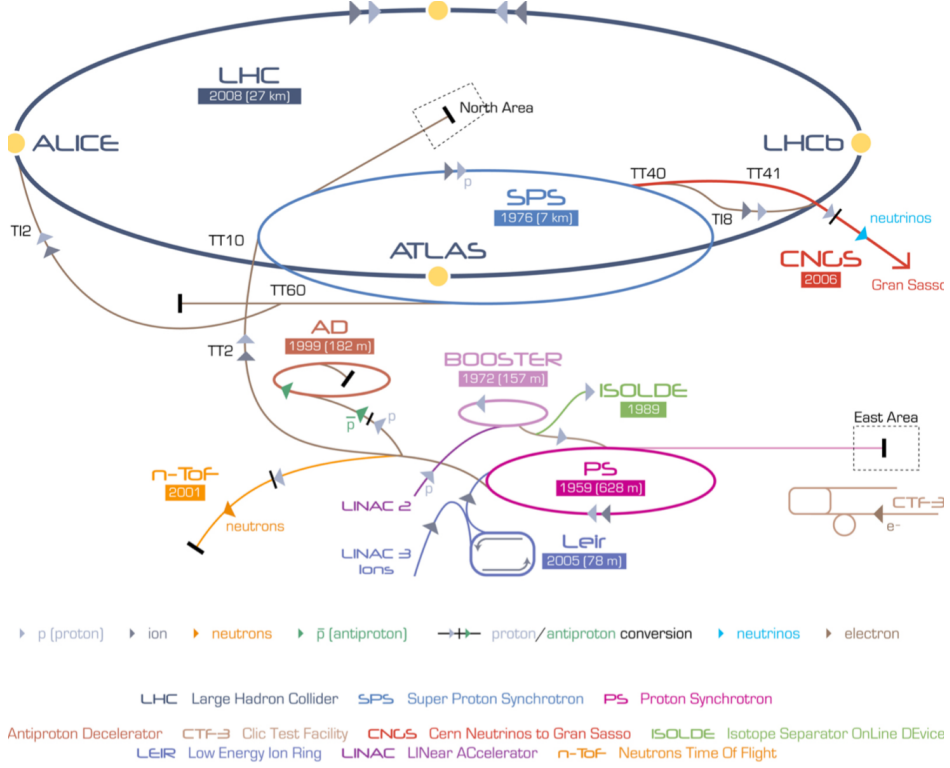


Figure 1.1: The CERN experiments and accelerators

features in 2015. All the data in this thesis was produced with the 2015 setup. For a more thorough review of the spectrometer see reference [1]. This chapter is roughly organized by how the data taking occurs and concludes with an extra section summarizing the unique features of the 2015 Drell-Yan data taking conditions.

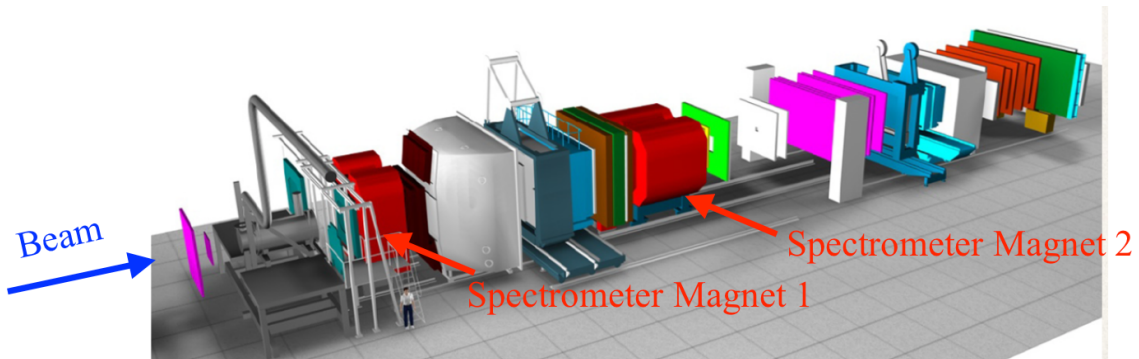


Figure 1.2: A schematic of the 2015 COMPASS setup

## 1.1 The Beam

The COMPASS spectrometer receives beam from the Super Proton Synchrotron along the M2 beam line. A schematic of the components in the M2 beam line is shown in Fig. 1.3. The SPS is the second largest accelerator at CERN with a circumference of almost 7 km which accelerates protons up to an energy of 450 GeV. The SPS extracts beam to famous Large Hadron Collier and as well sends beam to various experiments in the North Area at CERN. While the COMPASS spectrometer is above ground, the SPS is below ground and the M2 beam line must bend the beam from below ground to ground level.

There are several different beam types and energies available to COMPASS. The beam types used for physics analysis are a tertiary muon beam up to 190 GeV/ $c$  and secondary hadron beam with an energy up to 280 GeV/ $c$ . Both of the previous beam types can have a positive or negative charge. As well as the other two beam types it is also possible to have a low intensity tertiary electron beam, mainly used for calibrations.

The start of the M2 beam line is the T6 target. The SPS can accelerates primary protons up to 400 GeV/ $c$  to impinge on this T6 target which produces a secondary beam. The nominal proton intensity on the T6 target is  $100 \times 10^{11}$  spill $^{-1}$ . The T6 target is made of beryllium and has an adjustable length. The longer the T6 target the higher the secondary intensity where 500mm is the longest and typical target length used for physics data taking. The reaction of the proton beam with the T6 mainly produces secondary protons, pions and kaons. Following this reaction a series of dipole and quadruple magnets select the momentum and charge of interest.

The SPS spill structure varies throughout the data taking year depending mainly on the needs of the Large Hadron Colider (LHC). In 2015 the average intensity provided was  $0.6 \times 10^8$  s $^{-1}$  and the typical spill structure was two 4.8 second spills every 36 seconds.

### 1.1.1 Muon Beam

The muon beam is a tertiary beam which results from a weak decay of the secondary beam. After the initial proton reaction on T6 the resulting secondary particles are momentum and charge selected and sent through a 600m tunnel with focusing and de-focusing (FODO) quadruple magnets. In this tunnel the secondary pions and kaons can decay as

$$\pi^{-(+)} \rightarrow \mu^{-(+)} + \bar{\nu}_{\mu^-}(\nu_{\mu^+}) \quad (1.1)$$

and

$$K^{-(+)} \rightarrow \mu^{-(+)} + \bar{\nu}_{\mu^-}(\nu_{\mu^+}), \quad (1.2)$$

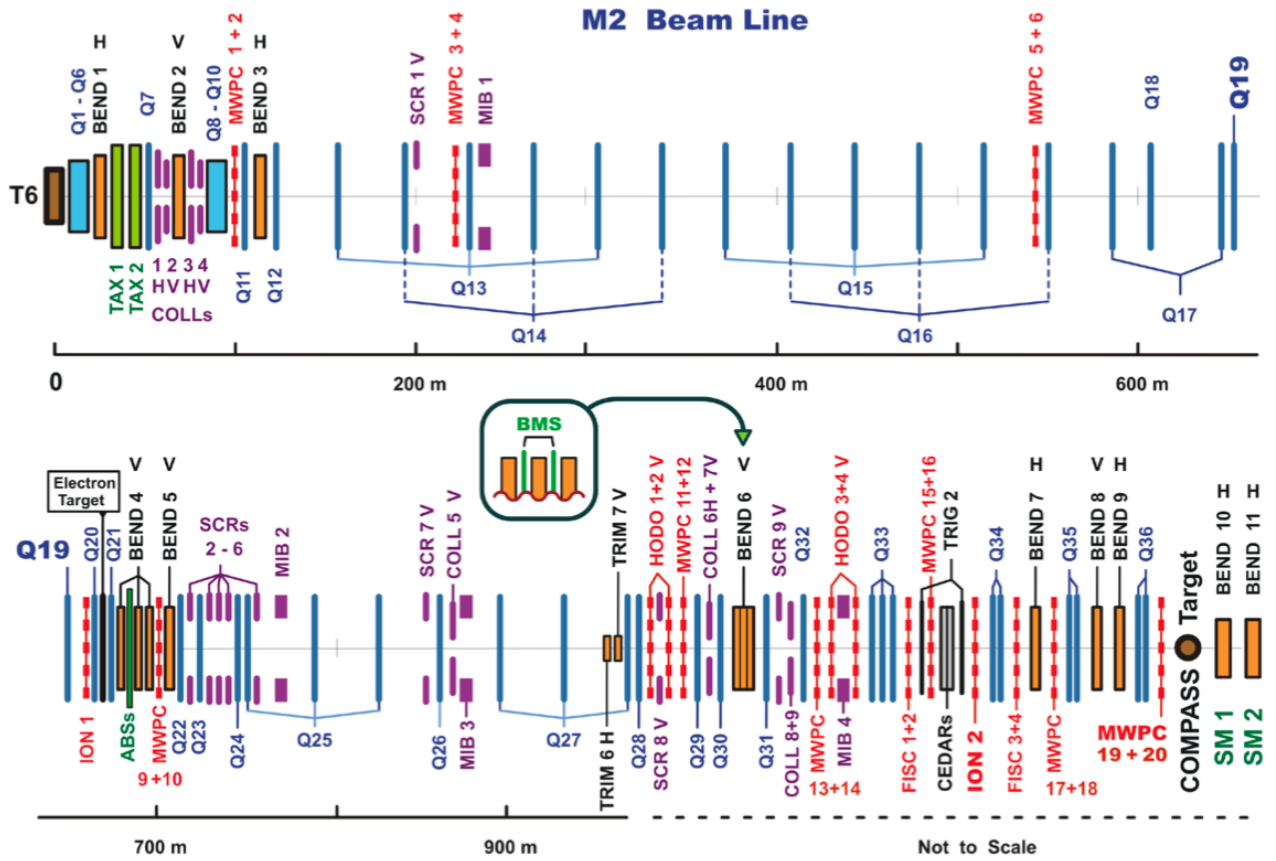


Figure 1.3: The M2 beam line at CERN

where  $K^{-(+)}$  is a kaon of negative or positive charge. At the end of the tunnel, a series of nine 1.1 m long beryllium absorbers, referred to as the ABS in Fig. 1.3, remove the remaining hadron component which did not decay. A 172 GeV/c secondary pion beam is chosen to achieve a 160 GeV/c tertiary muon beam. Due to the fact that the neutrino in the reactions 1.1 and 1.2 is always left handed, the muon will naturally be longitudinally polarized. For the muon momentum chosen, the muon beam achieves a polarization of 80%.

### 1.1.2 Hadron Beam

To deliver a hadron beam to COMPASS the ABS absorbers are not used. The decayed muons used for the tertiary muon beam have a lower momentum than the hadron beam and are therefore removable by magnetically rejecting these lower momentum muons. In the case of a negative hadron beam as in 2015, the composition of the beam is approximately 97 %  $\pi^-$ , 2.5% kaons and 0.5%  $\bar{p}$ . The 2015 Drell-Yan data taking was performed with a 190 GeV/ $c$  hadron beam.

### 1.1.3 Additional Beam Line Components

After the decay tunnel the beam is bent upwards along another FODO tunnel. The length of this tunnel is 250m and reaches the surface level approximately 100m before the COMPASS target. A series of three dipole magnets, called bend 6, then bend the beam to a horizontal position aimed at the COMPASS target. Both upstream and downstream of bend 6, there are three tracking detectors (BM01-BM06) that make up the Beam Momentum Station (BMS). The BMS is the upstream most component of the COMPASS spectrometer. It is able to determine the beam momentum to better than 1% of the beam momentum with an efficiency of approximately 93%. Bend 6 and the BMS are shown schematically in Fig. 1.4.

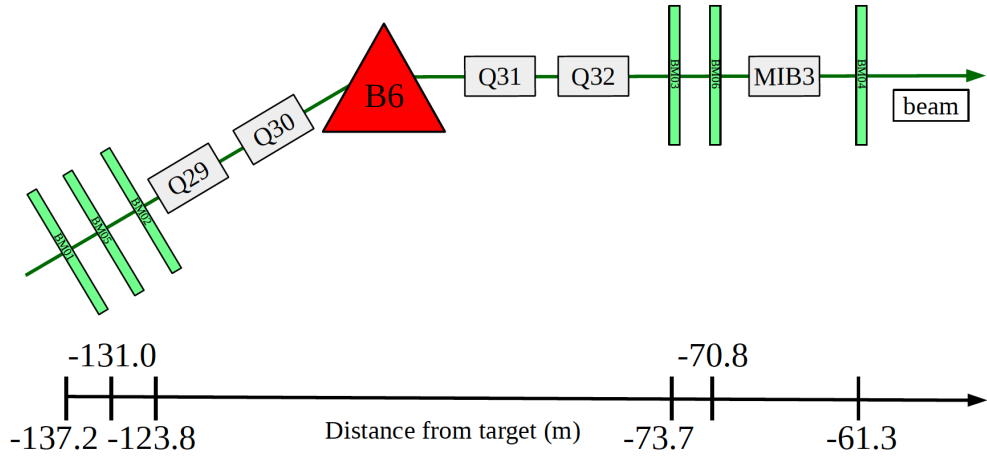


Figure 1.4: Bending the beam to a horizontal position. The BMS detectors are upstream and downstream of the bend 6 magnet.

During the 2015 Drell-Yan setup the  $\pi^-$  beam intensity was too high for the BMS station to work properly. For this reason, special low intensity, approximately  $10^6 \text{ s}^{-1}$ ,  $\pi^-$  beams were used in 2014 to determine the momentum distribution during Drell-Yan data taking. The beam momentum distribution is shown in Fig. 1.5 where the average momentum is 190.9 GeV/ $c$  with a spread of  $\pm 3.2 \text{ GeV}/c$ .

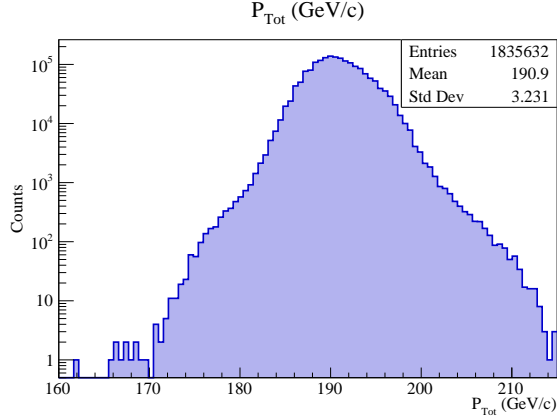


Figure 1.5: The momentum distribution of the  $\pi^-$  beam, determined during dedicated low intensity beam conditions

Approximately 30 m upstream of the target are two Cherenkov counter (CEDAR) detectors. As the hadron beam has contamination from several components these CEDARs can be used to distinguish between the different components. The CEDARs at COMPASS are high pressure detectors and have been demonstrated to achieve fast particle identification for particle momentums up to 300  $\text{GeV}/c$ . The CEDARs general principle of operation is that two particles with the same momentum but different mass will emit Cherenkov radiation at different angles relative to their momentum. When a particle is traveling faster than the speed of light in a given medium, it emits Cherenkov radiation in a cone centered along its momentum axis. The faster the particle is traveling the narrower the angle of the Cherenkov light cone. A schematic of the CEDAR operating principle is shown in Fig. 1.6. In 2015 the CEDARs were measured to be largely inefficient due to the high beam intensity and are not used for the analysis of this thesis.

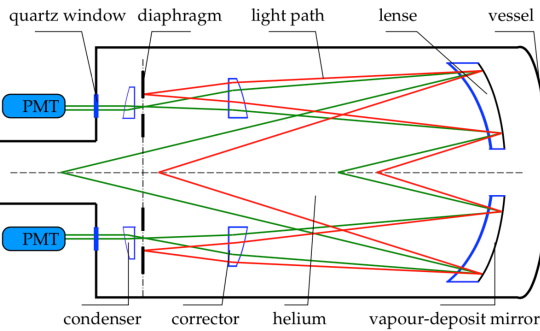


Figure 1.6: Light lines emitted inside CEDARs at COMPASS. The red(green) lines correspond to Cherenkov light emitted from a particle.

For years with a transversely polarized target, such as 2015, a chicane system of dipole magnets is setup in front of the target. The chicane first bends the beam away from the beam line and then back to the

target such that the beam hits the target at an angle. A chicane magnet setup is used because a beam hitting the target without any angle would then be deflected from the target magnet to the left or right of the spectrometer. For this reason the chicane gives the beam an angle before hitting the target such that the non-interacting beam exits the target traveling straight towards the spectrometer.

## 1.2 The Polarized Target

The polarized target at COMPASS is the most complicated and essential component of the spectrometer. It is located upstream of the tracking detectors and spectrometer magnets and downstream of the beam telescope, described in section 1.3, detectors. The target consists of two or three cylindrical cells. The possible materials are either solid state ammonia ( $\text{NH}_3$ ) or deuterated lithium ( ${}^6\text{LiD}$ ) or liquid hydrogen. Fig. 1.7 shows a schematic of the target.

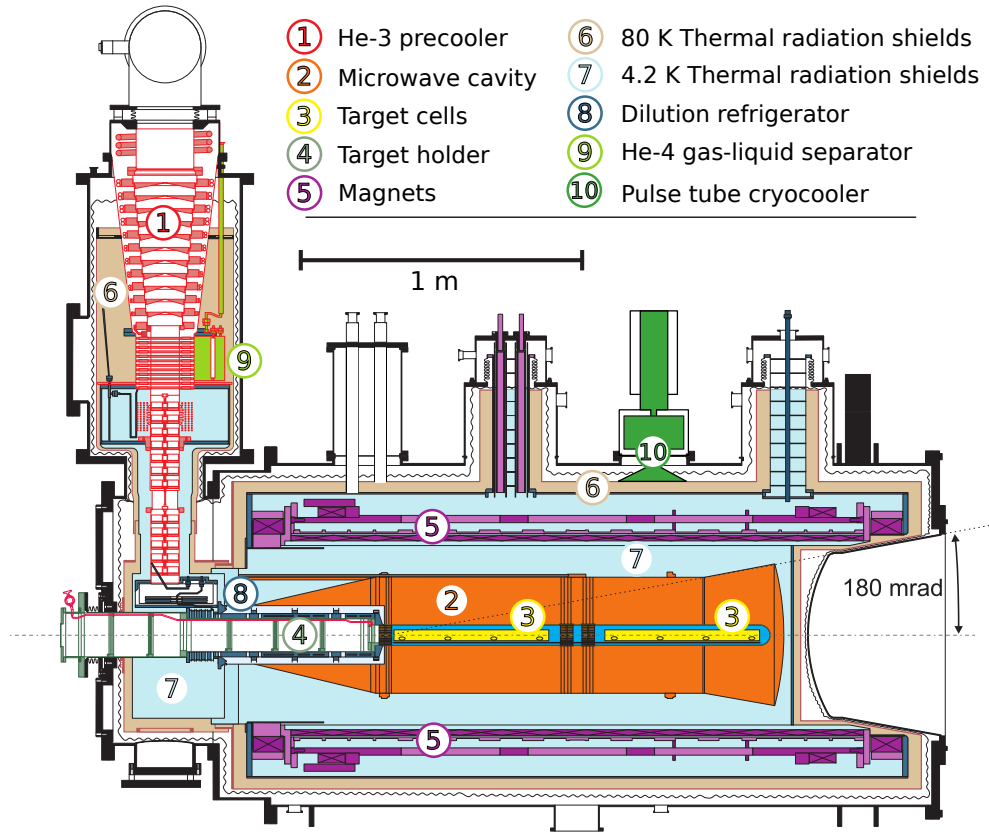


Figure 1.7: The polarized target at COMPASS

Surrounding the cylindrical cells is a longitudinal super conducting magnet capable of reaching a magnetic field of 2.5 T. This longitudinal magnet polarizes the target parallel or anti-parallel to the direction of the

beam momentum. The target polarization is maintained by keeping the target in a liquid helium bath of approximately 60 mK. This is called frozen spin mode where the temperature is maintained by a dilution refrigerator.

The target is polarized through the dynamic nuclear polarization (DNP) method [2]. This process works by first polarizing electrons in the target with the longitudinal magnet. With a high probability, the target electrons are all polarized in the same longitudinal direction for each target cells. Due to their much lower mass, electrons have a larger magnetic moment and therefore can be polarized at a much faster rate than protons or neutrons. At the same time the electrons are being longitudinally polarized, microwave electromagnetic radiation is sent through each target cell. For atoms which have a nuclear spin it is then possible for these atoms to absorb a microwave going to an excited state with the electron spin anti-parallel to the magnet and the nuclear spin either parallel or anti-parallel to the magnet depending on the microwave frequency. To ensure only one frequency enters each target cell, there is a microwave stopped between each target cell. The electron with the anti-aligned spin will then quickly have its spin realigned while the nucleon will take much longer to lose its polarization due to its smaller magnetic moment. This process can continue in this way resulting in a net nuclear polarization. Using the DNP method the target can achieve a polarization of approximately 90% in three days.

The target also includes a 0.63T transverse dipole magnet to change from longitudinal polarization to transversely polarized. The target must first be longitudinally polarized before the transverse target magnet can change the polarization direction. Once the target is transversely polarized, the target polarization can no longer be increased as microwaves can no longer shine on the target in the polarization direction. Therefore the polarization will decrease exponentially. In 2015 the target was polarized for about half a day between data taking sub-periods ad achieved an average polarization of 0.73%, including the effects of exponential polarization lose with time. The target transverse polarization relaxation time was about 1000 hours in 2015.

The target polarization was measured with 10 NMR coils while the target cells were longitudinal polarized. In the 2015, each target cell had the most upstream and downstream coils in the center of the target cell and the other three coils on the outside perimeter as is shown in Fig. 1.8. Due to the fact that the polarization can only be measured with the longitudinal magnet on, the polarization is only measure at the start and finish of a transversely polarized data taking. The intermediate polarization is then determined by exponential interpolating between these two times.

In 2015 the setup was two transversely polarized target cells of 55 cm length and 2 cm in radius. The cells were separated by 20 cm and polarized in opposite directions. The polarization of the target cells was flipped

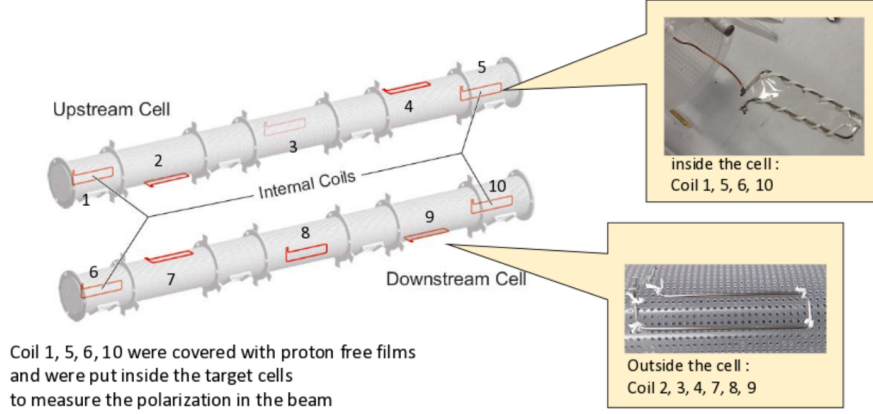


Figure 1.8: The empty polarized target cells side by side along with their NMR coil positions

ever two weeks of data taking to reduce systematic effects from luminosity and geometrical spectrometer acceptance. Due to the fact that the beam needs to be precisely steered onto the target and that the chicane magnets upstream of the target are setup for only one transverse target magnet direction, the transverse target magnet only pointed downward in 2015. To achieve a polarization flip the target polarization had to therefore be rotated back to the longitudinal direction and the input microwaves had to be changed to achieve the desired polarization direction.

The target material in 2015 was solid state NH<sub>3</sub>. The protons in the three hydrogen atoms were the only nucleons with nuclear spin and therefore only some fraction of the target was able to be polarized. The fraction of polarized nucleons to total nucleons is called the dilution factor. Counting the ratio of unpolarized nitrogen nucleons to polarized hydrogen, one would expect the dilution to be 3/17. However to get a more accurate determination of the dilution factor the follow calculation was used

$$f = \frac{n_H \sigma_{\pi^- H}^{DY}}{n_h \sigma_{\pi^- H}^{DY} + \sum_A n_A \sigma_{\pi^- A}^{DY}}, \quad (1.3)$$

where  $f$  is the dilution factor,  $n_H$  is the number of hydrogen atoms in NH<sub>3</sub>,  $n_A$  is the number of other nucleons in NH<sub>3</sub>, and  $\sigma_{\pi^- H}^{DY}$  and  $\sigma_{\pi^- A}^{DY}$  are the Drell-Yan cross-section for pion hydrogen scattering and

pion nucleon scattering respectively. The cross-sections were determined using a parton-level Monte-Carlo program MCFM [4]. The dilution factor was also further scaled down by studies of reconstruction migration between target cells. The average dilution factor in 2015 was determined to 0.18 in the invariant mass range of  $4.3(\text{GeV}/c)^2$  to  $8.5(\text{GeV}/c)^2$ .

## 1.3 Tracking Detectors

To determine when and where a reaction occurs in the polarized target, tracking detectors are able to position the products of the reaction. The goal of the tracking detectors is to determine a point in space where a particle traversed. The COMPASS tracking detectors attempt to do this for a wide range of angles, momentums and at different rates. For these reasons there are several planar tracking technologies used at COMPASS which can be divided into three categories: very small angle tracker, small angle trackers and large area trackers. As the name suggest very small angle trackers measure tracks with small angle deflections from the beam axis which are essentially beam particles. The small area trackers measure particle tracks with low but non-zero scattering polar angle and have small central dead zones. The large area trackers are several meters in height and width and measures the largest deflection angles up to 180 mrad.

All of these trackers are split into stations. Each station corresponds to several detectors planes at roughly the same z-position along the beam line. Each station measures a track position in one or more orientation while most measure tracks in three or more orientations. The coordinate orientations measured are the X and Y coordinates which are the horizontal and vertical directions respectfully, and as well the U and V coordinates which are rotated at different angles with respect the X and Y coordinates.

### 1.3.1 Very Small Angle Trackers

The very small angle trackers extend up to 3 cm away from the beam axis. This is the region with the highest number of tracking particles and therefore these detectors must be able to handle the highest rates up to  $5 \times 10^7$  Hz. The two detector types that make up the very small angle trackers are either scintillating fiber detectors (SciFi) or silicon microstrip detectors. These two detector types are complementary to each other as the former have very good timing resolution while the latter have very good spacial resolution.

There are three silicon stations possible at COMPASS. These stations have active detecting areas of  $5 \times 7 \text{ cm}^2$ . The spacial resolution of these detectors is nominally  $10 \mu\text{m}$  and the timing resolution is nominally 2.5 ns. For the 2015 setup, the beam intensity was too high for the silicon detectors to operate and therefore these detectors were not used.

There are 10 SciFi stations available at COMPASS. The active areas vary from  $3.9 \times 3.9 \text{ cm}^2$  to  $12.3 \times 12.3 \text{ cm}^2$  planar areas. As well the detection fiber diameters vary between detectors with the different diameters used at COMPASS being 0.5 nm, 0.75 nm and 1 nm. Several fibers are bundled together to determine a strip hit position and the resulting nominal spacial resolutions are  $130 \mu\text{m}$ ,  $170 \mu\text{m}$  and  $210 \mu\text{m}$ . The nominal timing resolution of these detectors is about 400 ps. In 2015 three SciFi stations made up the beam telescope and were placed upstream of the target to measure the beam trajectory and timing information. A fourth SciFi station was place in the LAS section of the spectrometer.

### 1.3.2 Small Angle Trackers

The small angle trackers detect particles with non-zero deflection angles. These detectors have medium size active areas compared to the very small angle trackers and the large angle trackers. They cover 5 cm to 40 cm from the beam axis where the rate drops to approximate  $10^5 \text{ Hz}$ , two orders of magnitude lower than the rates the very small angle trackers receive. At COMPASS there are two types of small area tracking detectors: micromesh gaseous structure (micromegas) and gas electron multipliers (GEMs).

There are three micromega stations at COMPASS. All three stations are location sequentially after each other between the target and the first spectrometer magnet. As well all three detectors measure four coordinate projections and have an active area of  $40 \times 40 \text{ cm}^2$  with a 5 cm diameter dead zone. The micromegas operate by having a conversion region and a smaller amplification region. An ionized particle produced in the conversion region will drift through an electric field of around  $3.2 \text{ kV/cm}$  to the amplification region where the electric field is around  $50 \text{ kV/cm}$ . The electric field is too small for amplification in the conversion region but as the name suggest the electric field is high enough to amplify the signal in the amplification region. The amplified signal is then read out on strips. The conversion and amplification regions are separated by a metallic micromesh material. The electrons pass through the micromesh without resistance and are not rimmed out. The micromegas have good spacial resolution because the thickness of the amplification region is only  $100 \mu\text{m}$ , small enough to prevent much transverse spreading of the electron avalanche between strips. The separation of the larger conversion region from the smaller amplification region with the micromesh prevents electric field lines from being distorted in the conversion region and therefore prevents the primary electrons from drifting slower in the conversion region. This allows micromegas to operate at a higher rate than would be possible otherwise. This principle of operation is illustrated in Fig. 1.9. The strips in the central part of the detector are  $360 \mu\text{m}$  corresponding to a resolution of about  $100 \mu\text{m}$  and the strips in the outer region are  $460 \mu\text{m}$  corresponding to a resolution of about  $120 \mu\text{m}$ . The nominal timing resolution 9 ns. In 2015 the micromegas were upgraded to include a pixelized section covering much of the dead zone area.

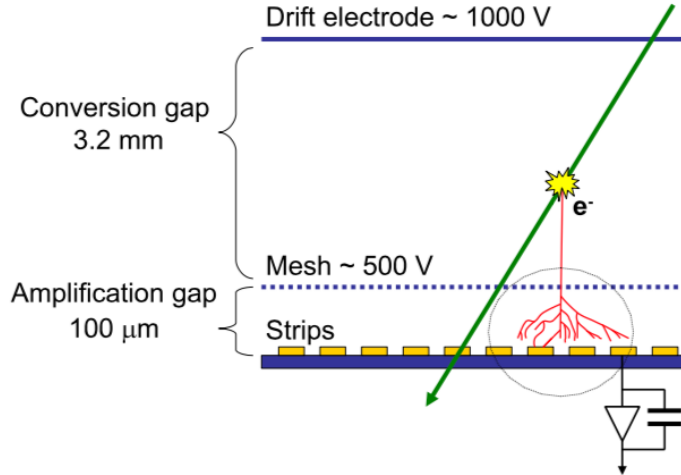


Figure 1.9: Principle of operation for the micromesh gaseous structures (micromegas)

There are eleven GEM detectors located throughout the COMPASS spectrometer. The first GEMs are located after the first spectrometer magnet and the last GEMs are located near the end of the spectrometer. These detectors are positioned close to the beam axis. They are mounted on a large area tracker, covering the dead zone region of the large area tracker. All eleven detectors have an active area of  $31 \times 31 \text{ cm}^2$  and a 5 cm diameter dead zone. In times of lower beam intensity the dead zones can be turned on as an active area.

The detector is split into four regions. These regions are separated by a polyimide foil (50  $\mu\text{m}$  thick) having around  $10^4 \text{ cm}^{-1}$  drifting holes of 70  $\mu\text{m}$  diameter and are clad with copper on both sides. There is an electric potential of a few hundred volts between each foil layer. The electron amplification occurs around the holes of each of the three foil dividers. This means GEM detectors speed up the amplification process by splitting the amplification avalanche into three locations. The process is sped up because the drifting electrons are accelerated multiple times thereby speeding up their drifting velocity which therefore reduces the overall drift time from the ionization location to the strip readout. This allows the GEMs to operate at a higher rate than would otherwise be possible. The principle of operation is illustrated in Fig. 1.10. The nominal timing and spacial resolution of the GEM detectors is 10 ns and 110  $\mu\text{m}$  respectively. Two pixelized GEM detectors were also in operation but were not as crucial for the 2015 Drell-Yan measurement.

### 1.3.3 Large Area Trackers

The large area trackers measure the largest polar scattering angles at COMPASS. Their dead zones mostly coincide with a small area tracker, described in the previous section 1.3.2, which therefore means these

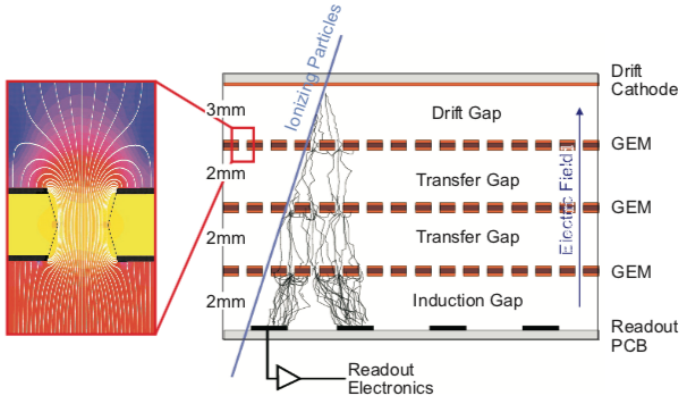


Figure 1.10: The operation principle of the gas electron multiplier (GEM) detectors

detectors do not have to process the higher fluxes very close to the beam line. The most important feature of these detectors is that they have a large planar area. As a consequence however, their position and timing resolutions are not as good as the small and very small angle trackers. The types of large area trackers used at COMPASS are all gaseous detectors and include drift chambers (DCs), straw tube detectors (straws) and multi-wire proportional chambers (MWPCs).

The first four drift chambers downstream of the target are named DC00, DC01, DC04 and DC05. The first two, DC00 and DC01, have smaller active areas of  $180 \times 127 \text{ cm}^2$  and a circular dead zone of 30 cm diameter. These two drift chambers are positioned upstream of the SM1 magnet. The rates upstream of SM1 are higher. This is due to the fact that low energy particles are produced in the target, but are bent out of the acceptance of spectrometer by SM1. Therefore detectors downstream of SM1 do not track these low energy particles and therefore DC00 and DC01 need to be able to process a higher particle flux. The next two drift chambers, DC04 and DC05, are downstream of SM1 and both have larger active areas of  $240 \times 204 \text{ cm}^2$  and as well have dead zones of 30 cm diameter. The active areas of all four of these DCs was roughly chosen to coincide with the acceptance of the SM1 yoke. DC05 was first installed for the 2015 Drell-Yan data taking and is further described in chapter ???. All four of these DCs measure four projection views corresponding to eight detector layers. A sketch of the principle of operation is shown in Fig. 1.11. The nominal spacial resolution for these detectors is  $250 \mu\text{m}$ .

Further downstream the spectrometer, downstream of the SM2 magnet, are the W45 drift chamber stations. The W45 drift chambers are the largest drift chambers at COMPASS. There are six W45 detector stations which each have an active area of  $520 \times 260 \text{ cm}^2$  and a circular dead zone of 50 cm or 100 cm diameter.

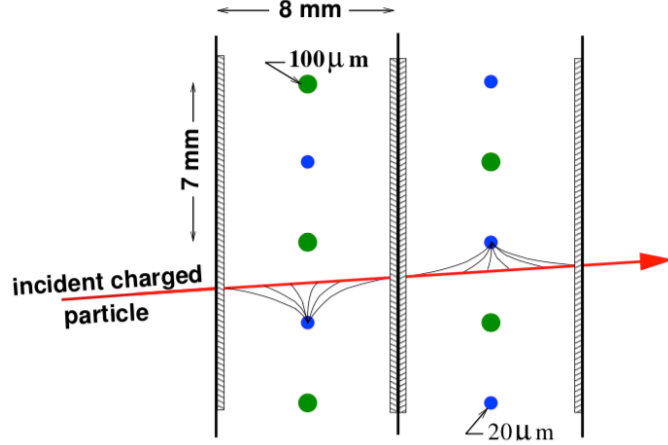


Figure 1.11: Drift cell of a drift chamber with the ionized drift electron lines coming from the incident charged particle

Each W45 station measures two projection views corresponding to four detector layers. The drift cells in W45 are 40x10 mm<sup>2</sup> and the spacial resolution is nominally 1500  $\mu\text{m}$ .

The two straw stations in operation during the 2015 data taking are named ST03 and ST05. ST03 was in the large angle spectrometer after DC05 and consisted of two stations measuring six projection views. ST05 was in the small angle spectrometer and measured three projection views. The active areas of each of the horizontal wire stations is 350x243 cm<sup>2</sup> and the active area of each of the rotated wires is 323x272 cm<sup>2</sup>. The principle of operation for the straw detectors is very similar to that of a drift chamber. However, instead of having the detector made up of connected drift cells the straw detectors are made of separated circular tubes. Each tube consist of a gold plated tungsten anode wire in the center and the walls of the tube make up a cathode. Due to the fact that the cathode completely surrounds the anode wire there is no electrical interference between neighboring anode wires as there is for drift chambers. For this reason the electric field in each tube is easier to control and the ionized electron drift speed is more linear than other detectors. Each straw detector plane is divided into sections where the straw tubes in the outer most section from the beam line have a diameter of 9.6 mm and the tubes close to the beam line have a diameter of 6.1 mm. In addition, in the central part of the detector there is a physical hole, dead zone of 20x20 cm<sup>2</sup>. The nominal position resolution for these detectors is 400  $\mu\text{m}$ . A frontal schematic is shown in Fig. 1.12. For the reason that most of the detected muons are reconstructed in the large angle spectrometer and the fact that many of the high voltage modules were not operation for ST05 in 2015, ST05 was not used for track reconstruction for 2015 Drell-Yan data.

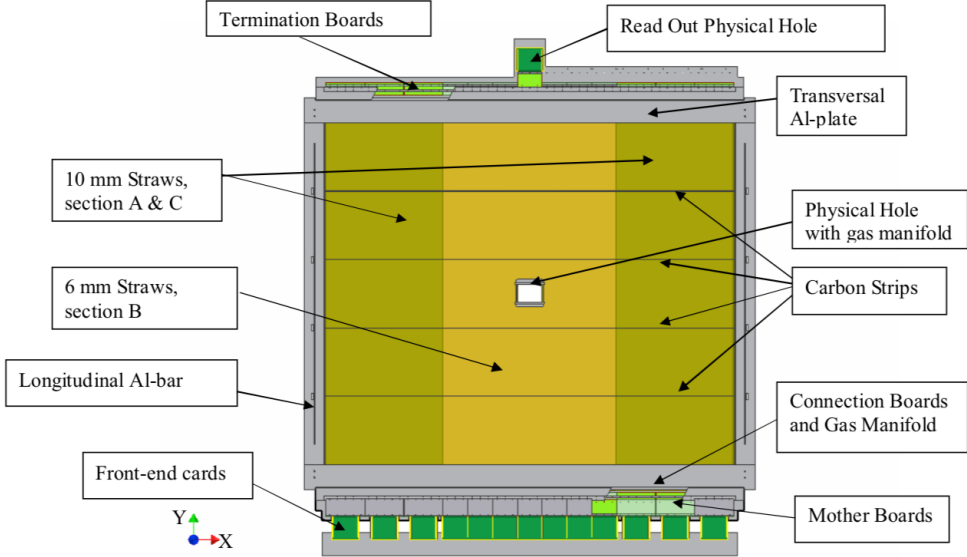


Figure 1.12: Front on view of the active area of a straw detector at COMPASS

The next type of large angle track is the richwall. This large area tracker operates similarly to the straw tube detectors. The detector consist of eight layers of mini drift tubes (MDT) shown in Fig. 1.13. The central part of each MDT includes a gold plated tungsten sense wire. The richwall is located before the SM2 magnet and after ST03 with an active area of  $5.27 \times 3.91 \text{ cm}^2$  and a central dead zone of  $1.02 \times 0.51 \text{ cm}^2$ . The nominal position resolution of this detector is  $600 \mu\text{m}$ .

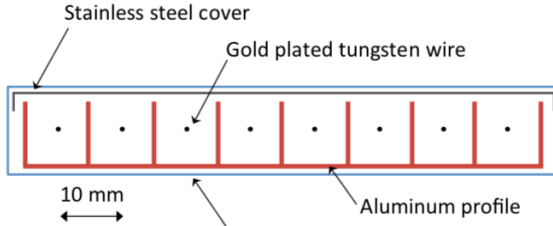


Figure 1.13: The richwall mini drift tubes

The final type of large area tracking detector at COMPASS is the MWPC. There are 14 of these stations located throughout the experiment. The MWPCs are separated into three categories distinguished by the coordinates they measure. The first type is called type A and consists of three projection views measuring an x, u and v coordinate. The second type is type A\* and is the same as type A but measures the y coordinate in addition to the other three coordinates. Both type A and A\* have active areas of  $178 \times 120 \text{ cm}^2$ . The final type is type B which has a smaller active area of  $178 \times 90 \text{ cm}^2$  and measures the same projections as type A.

There are seven stations of type A, one station of type A\* and six stations of type B. All three types have circular dead zones of diameters 16 cm, 20 cm and 22 cm for types A, A\* and B respectively.

The MWPCs operate on similar principles to the drift chambers but without a calibration drift curve. For this reason the MWPCs can be made to have one common gas volume between each station. Their position resolution is determined as

$$\frac{\text{sense wire separation}}{\sqrt{12}}, \quad (1.4)$$

which is the variance of a uniform distribution. The separation between sense wires is approximately 2 mm which corresponds to a spacial resolution of these detectors of around 600  $\mu\text{m}$ .

## 1.4 Particle Identification

In the COMPASS spectrometer there are four types of detectors used to determine particle identification (PID). These four detectors are the ring image Cherenkov (RICH) detector, electromagnet calorimeters (ECAL), hadron calorimeters (HCAL) and muon walls (MW). The RICH distinguishes between pions, kaons and protons; ECAL1 and ECAL2 measure the energy from photons and electrons; HCAL1 and HCAL2 measure the energy from hadrons; and MW1 and MW2 distinguish muons from all other particles. The RICH, ECAL1, HCAL1 and MW1 are in the large angle spectrometer in that respective order along the beam line. The small angle spectrometer includes ECAL2, HCAL2 and MW2 again in that respective order along the beam line.

The RICH detector operates similarly to the CEDARS, section 1.1.3. In the RICH, Cherenkov radiation is emitted from particles traveling through it at an angle dependent on the particle's velocity. The RICH is filled with a dielectric gas,  $\text{C}_4\text{F}_{10}$ , which has an index of refraction greater than air. The momentum of a particle going through the RICH is determined from bending radius around SM1. Therefore once the RICH determines the entering particle's velocity, the mass of particles can be distinguished. A sketch of the RICH and its operating principle is shown in Fig. 1.14. To distinguish between particles the minimum momenta are: 2.5  $\text{GeV}/c$  for pions, 9  $\text{GeV}/c$  for kaons and 17  $\text{GeV}/c$  for protons. The maximum momentum the RICH can distinguish between any of these particles is 50  $\text{GeV}/c$ . This detector is located in the large angle spectrometer before any calorimeters.

The ECALs and HCALs both measure the energy of entering particles. Both types of calorimeters do this by stopping a specific entering particle, where the amount of energy deposited in each respective calorimeter is proportional to the incoming particle's energy. ECALs are able to stop and measure electron and ph-

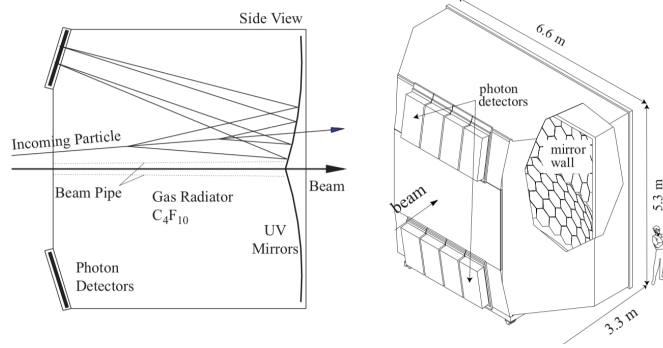


Figure 1.14: Side view demonstrating the principle of operation of the RICH detector.

ton energies and HCALs stop and measure hadron energies. The energy knowledge along the momentum determined from the tracking detectors allows the ability to determine the particle's identification.

The ECALs are made of lead glass towers with photon multipliers attached to these towers on one side. An incoming photon or electron interacts with the lead glass to produce a light signal which is readout with these photon multipliers. Other particles also interact with the material in the ECALs however hadrons and muons are able to exit through the detector unlike photons and electrons. A frontal view of ECAL1 is shown in Fig. 1.15 and a frontal view of ECAL2 is shown in figure Fig. 1.16.

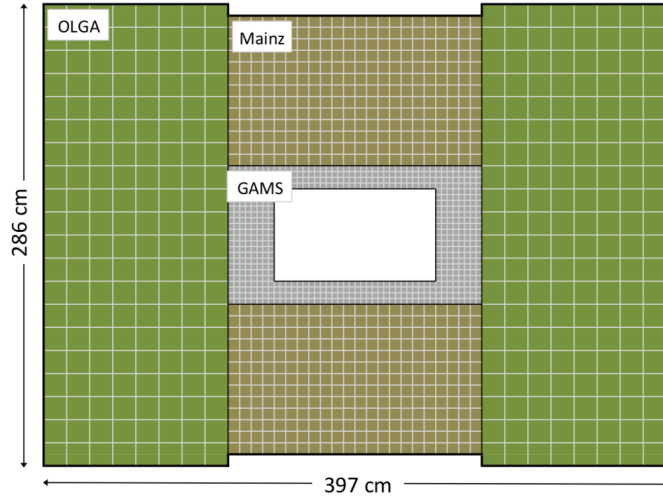


Figure 1.15: Frontal view of the electromagnetic calorimeter 1

The HCALs are sampling calorimeters which are made of alternating layers of iron and scintillating material. An incoming hadron deposits all its energy in the HCAL by making a particle showers in the iron. This particle shower makes a signal in the scintillating material which is then read out by photo multipliers. The HCALs are placed after the ECALs in each stage of the spectrometer because an electromagnetic shower

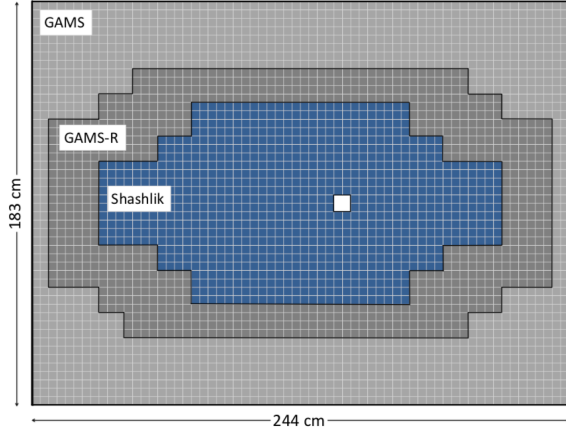


Figure 1.16: Frontal view of the electromagnetic calorimeter 2

happens within less material budget than a hadronic shower. The HCALs are effect at determining particle energies from particle with energies between 10 GeV and 100 GeV.

The two MWs are located after an HCAL in their respective stages. Due to their higher mass and absence of color charge, muons are able to pass through the most material budget of any of the particles detected at COMPASS. For this reason both MWs consist of an absorber and tracking detectors downstream of this absorber. Any particles that make it through the absorber are with a very high probability muons.

MW1 consists of eight tracking planes before a 60 cm iron absorber and the same number of tracking planes after this absorber. The tracking portions of MW1 are built similarly to the richwall, described in section 1.3.2, in that they are also made of MDT modules. The active area of MW1 is  $480 \times 410 \text{ cm}^2$  and includes a dead zone of  $140 \times 80 \text{ cm}^2$ . Each plane of this detector has a spacial resolution of 3 mm. A sketch of MW1 is shown in Fig. 1.17.

The second muon wall, MW2, is located downstream of a 2.4 m thick concrete absorber. MW2 consists of 12 planes each with an active area of  $450 \times 450 \text{ cm}^2$  and a dead zone of  $90 \times 70 \text{ cm}^2$ . The detector operates similarly to the straw detectors, section 1.3.2, in that the detector is made of drift tubes with a wire in the center of these tubes. The diameter of the drift tubes is 29 mm and the position resolution is about 1.4 mm.

There is one last absorber in the COMPASS spectrometer located before the H5 hodoscope at the end of the spectrometer hall. This absorber is called muon filter 3 (MW3) and ensures that the inner trigger is only triggered by a muon.

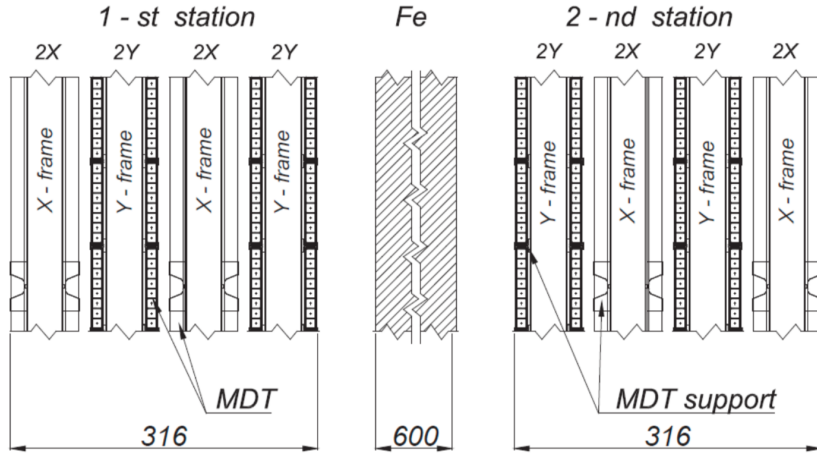


Figure 1.17: A side view sketch of the muon wall 1 detector

## 1.5 Trigger

The trigger system at COMPASS defines what is an event. Whenever the trigger signal is given, all the detector information within a few nanosecond timing window is recorded. Due to the fact that there are very many background events occurring as the beam impinges on the target, there is too much information going to the front end modules (FEMs) of the detectors for the FEMs to process and record all this information. For this reason only a certain subset of all the information is stored to disk. The trigger system must therefore have good timing resolution to make quick decisions on which data to record. At COMPASS the trigger systems consist of scintillating hodoscopes attached to PMTs. The timing resolution of these detectors is approximately 1 ns. A top view schematic of COMPASS showing where the relative positions of the hodoscopes for each trigger is shown in Fig. 1.18.

At COMPASS there are five different triggers used to register physics events. Each trigger type includes at least two hodoscopes at different z-positions in the spectrometer. The types of triggers are either target pointing, when the hodoscope slabs are horizontal; or energy loss, when the hodoscope slabs are vertical. The target pointing trigger is setup and used with higher polar scattering angles. As the name suggest, this trigger signals when a particle is scattered from the target. The energy loss trigger is used to trigger on lower  $Q^2$  interactions and signals when a particle is bent a specified amount. This concept is illustrated in Fig. 1.19.

There are four triggers in SAS: the inner trigger (IT), the middle trigger (MT), the ladder trigger (LT) and the outer trigger (OT). The IT is an energy loss trigger and includes the hodoscopes HI04X and HI05X. The MT includes both energy loss and target pointing slabs. The hodoscopes in the MT are HM04X,

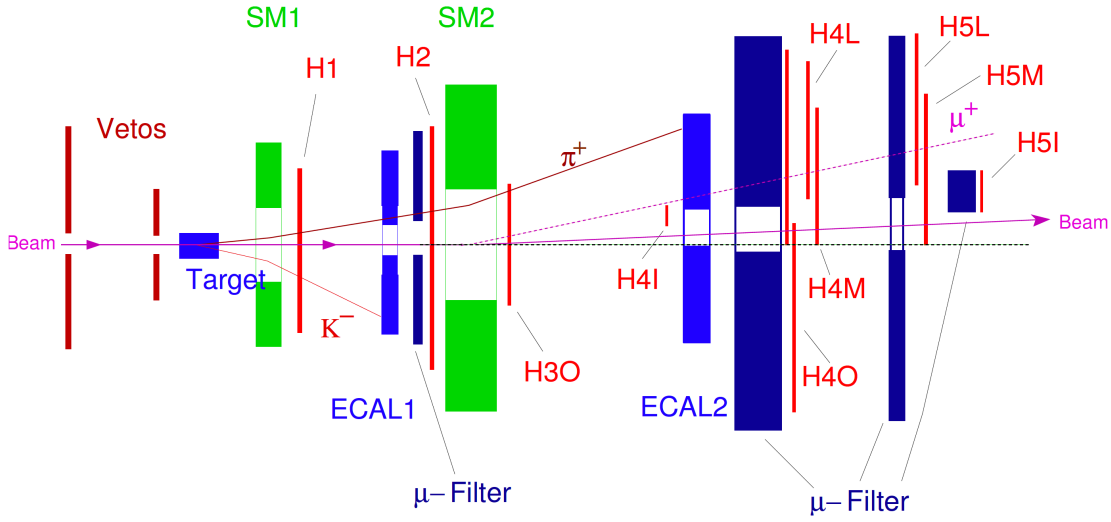


Figure 1.18: Top view of the spectrometer highlighting how different particles can signal a trigger

HM05X, HM04Y and HM05Y. The MT hodoscopes whose names end with an X have vertical slabs and those ending with a Y have horizontal slabs. The LT is an energy loss trigger which consists of HL04X and HL05X. The final trigger in SAS, the OT, is a target pointing trigger and consists of hodoscopes HO03Y and HO04Y. The remaining trigger system is in LAS and is a target pointing trigger consisting of hodoscopes HG01Y and HG02Y. The kinematic coverage for the 2015 triggers is shown in Fig. 1.20.

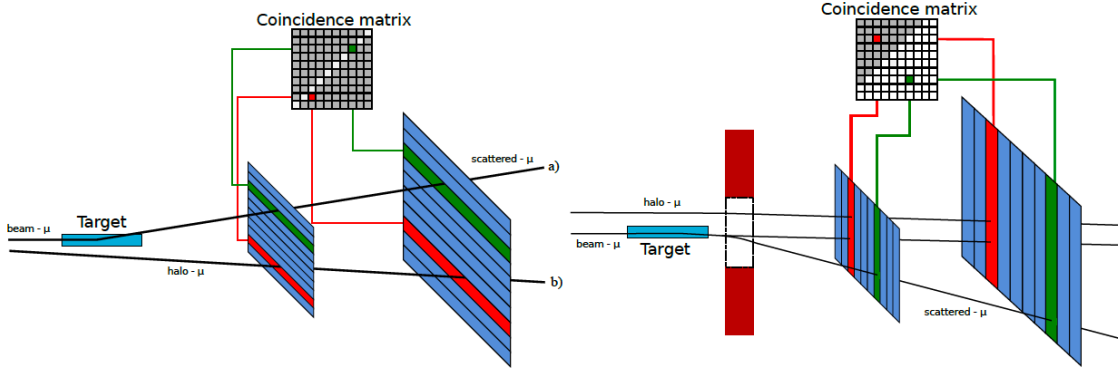


Figure 1.19: The two types of triggers (left is target pointing and right is energy loss) at COMPASS and an illustration of the coincidence matrix used to select events of interest

In addition to signaling when interesting events occur, it is also important to signal when background events are occurring. For this reason there is also a veto system upstream of the target as shown in Fig. 1.18. This veto trigger consists of hodoscopes attached to PMTs as well. It is centered on the beam axis but has hole center on the nominal beam line. The veto trigger is used to reject halo muons which surround the beam.

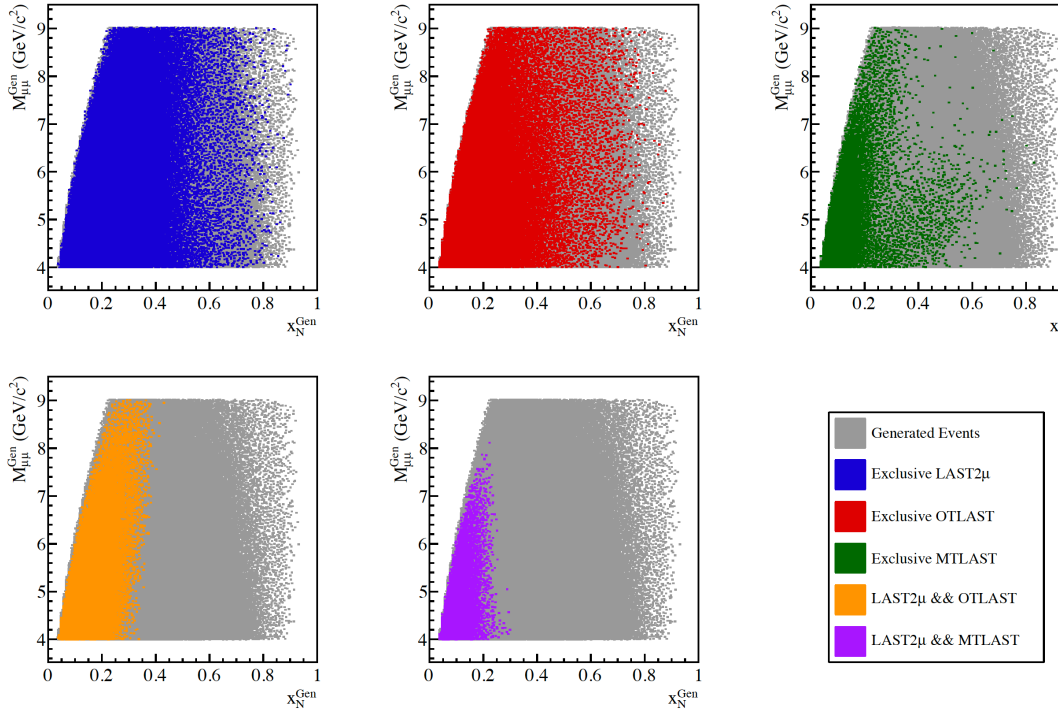


Figure 1.20: The kinematic coverage for the 2015 triggers determined from Monte-Carlo studies

Halo muons result from the beam decaying, as in Eq. 1.1 and Eq. 1.2, where this decay occurs upstream of the target but downstream of the ABS absorbers. The muon halo surrounds the hadron beam due to the muon's lower momentum, and it is for this reason that the veto hodoscopes, outside of the beam line, are able to reject events that would occur due to the halo.

There is one trigger in the spectrometer hall that is not a hodoscopes. This is the calorimeter trigger (CT). The CT can be used as a trigger when a particle deposits more than a certain energy threshold in the specified calorimeter. In 2015 this trigger was only used as an independent study of the other triggers at COMPASS. Particularly the CT was used to measure the trigger hodoscopes efficiencies.

The last trigger used at COMPASS is a random trigger. This trigger is setup outside of the spectrometer area and registers a signal when a radioactive source disintegrates. In this way the random trigger is truly random. In 2015 this trigger was used in studies of the beam flux.

In 2015, the goal was to measure two muons in the spectrometer. For this reason, two triggers must each signal a particle in coincidence for an event to be registered. For physics analysis the coincidence triggers are either two muons in LAS (LASxLAS), one muon in LAS and one in the OT (LASxOT) or one muon in LAS and one muon in the MT (LASxMT). The LASxLAS trigger system covers the high  $Q^2$  and high  $x_{\text{beam}}$  phase space whereas the triggers including a SAS hodoscope cover lower  $Q^2$  values. In addition to

these three dimuon triggers where three single muon triggers corresponding to a particle in LAS, MT or OT. These three single muon triggers, however, were pre-scaled down to only take every 500, 100 or 100 events respectively. For further tests 2015 included a random trigger and a beam trigger pre-scaled down by 35000.

## 1.6 Data Acquisition

The data acquisition (DAQ) collects data from the over 250,000 detector channels and transfers this data to storage on magnetic tape at CASTOR (CERN Advanced STORage). Despite the triggering system used to reduce the data rate, the data still is recorded at event rates between 10 kHz to 100 kHz. A typical COMPASS event size is 45 kB. The DAQ is designed to process these data rates and size while minimizing the dead time associated with data collection and transfer. In 2015 the dead time was approximately 10%. The total data the DAQ recorded, after the spectrometer finished commissioning, was approximately 750 terabytes of raw data.

Data collection begins with the digitization of information from a detector channel. This digitization is performed by a time to digital converter (TDC) or an analogue to digital converter (ADC). These TDCs and ADCs are either on the detector FEMs or on custom COMPASS readout electronics named: GANDOLF (Generic Advanced Numerical Device for Analog and Logic Functions), GeSiCA (Gem and Silicon Control and Acquisition) or CATCH (COMPASS Accumulate Transfer and Control Hardware). After digitization the data is transferred by optical fibers to an FPGA multiplexer where the data is buffered by spill and arranged by event. From there an FPGA switch sends the data to multiplexer slaves. The slaves are online computers that oversee the final steps for raw data and transfer this data to CASTOR. This whole process is shown schematically in Fig. 1.21.

## 1.7 Data Reconstruction

The COMPASS Reconstruction and AnaLysis Program (CORAL) reconstructs the raw data into physical quantities. For example CORAL is able to convert the raw data into particle tracks with momentum, charged and possibly an originating vertex location [3]. The raw data from the DAQ is digitized timing information from tracking detectors or digitized energy information for calorimeters. The process of reconstructing tracks takes the detector timing information and determines a position in space for a particular tracking detector based on a calibration. CORAL then uses a Kalman Filter to determine straight tracks in regions with no or low magnetic field [5]. The tracks are then connected through the magnetic field using a fast lookup table for known possible bending radii. At this point a track is determined to have a momentum, charge and a  $\chi^2$

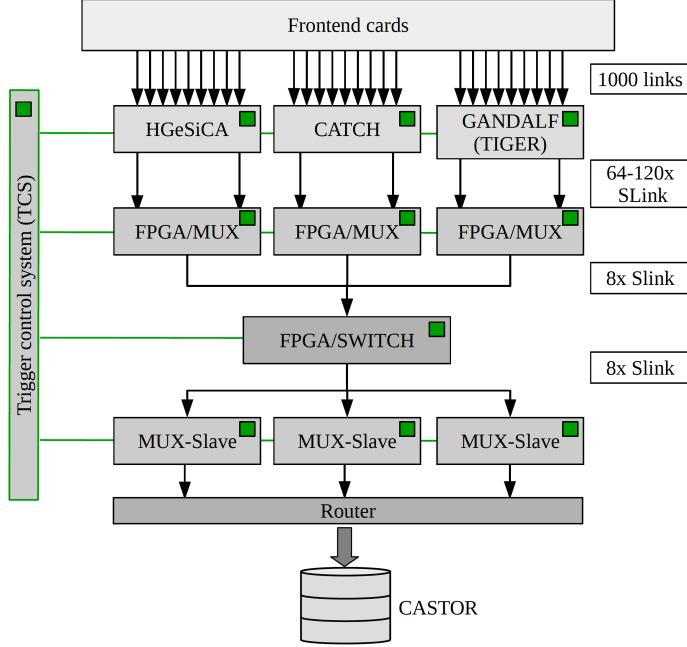


Figure 1.21: The data acquisition steps at COMPASS

value associated with the track. From there the tracks are extrapolated back to the target region and the intersection of at least two tracks is determined as a vertex. If in addition to the two intersecting tracks, a beam particle can be extrapolated forward to the same vertex location then the vertex is assigned to be a primary vertex. Otherwise the vertex is defined as a secondary vertex.

This reconstruction stage reduces the data volume by approximately a factor of 10. A diagram of the reconstruction data flow is shown in Fig. 1.22. In 2015 there were several data reconstructions performed. Between each reconstruction improvements were made to detector calibrations, detector alignment, beam tracking and any other preprocessing improvements that could be made. The final two productions are the t3 production and the slot1 production. The results shown in this thesis are from either t3 or slot1 productions.

Once reconstruction has been performed the data is stored in data structured trees (DSTs). The usual procedure of reconstruction which gives physical values such as momentum and charge to tracks, results in data called miniDSTs. There is also the possibility to save more information, for example detector hit location information, to make so called fatDSTs. These DSTs are now in a format which can be processed by PHAST (PHysics Analysis Software Tool). PHAST is a COMPASS program written to further analyze physics data. With PHAST there is the possibility to loop over all the miniDSTs and make certain cuts and to produce a so called  $\mu$ DSTs based on these cuts. In 2015  $\mu$ DSTs were made for all the analysis data

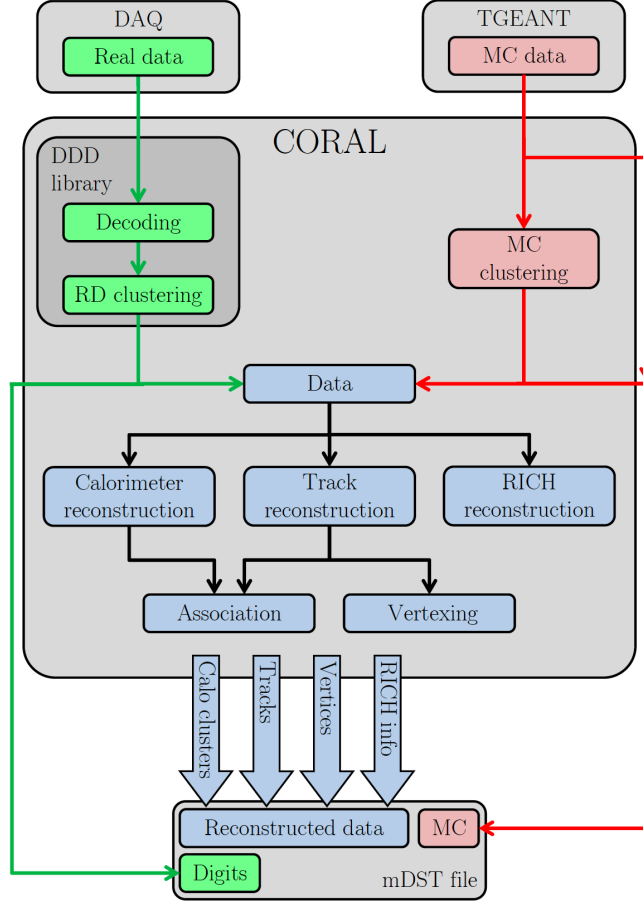


Figure 1.22: The schematic of the CORAL reconstruction process

where a cut was applied to the miniDSTs saving only events with at least two muons. Both CORAL and PHAST are fully object-oriented C++ programs.

### 1.7.1 Monte-Carlo Production

Monte-Carlo data is simulated data which is performed in three steps. First a programs generates specific physics processes based on their theoretical probabilities. The generators of Monte-Carlo used for this thesis are PYTHIA versions 6 and 8 [6]. Next a GEANT4 simulation of COMPASS determines if a detector will register a hit from these generated physics processes. This saves the data in a raw data format which can be reconstructed by CORAL. Finally the simulated data is reconstructed by CORAL and analyzed in PHAST the same as if the data were real data.

## 1.8 2015 Drell-Yan Data Taking

The 2015 Drell-Yan data taking is one of the main programs for the COMPASS-II experiment. The data taking began in April of 2015 and ended in November of that year. The physics data used for analysis started in July and finished at the end of data taking. The data recorded before July was used for calibrations and commissioning. The total analysis data was split into nine data periods labeled W07-W15 where each data period corresponded to approximately two weeks of beam time. The spin orientation of each target cell was reversed after the first week of every period to reduce systematic effects arising from different geometric acceptances and luminosities of the up and downstream target cells.

### 1.8.1 Hadron Absorber

The previous sections in this chapter described the spectrometer setup generally and mentioned the specifics for the 2015 setup. The main unique hardware addition in 2015 is the hadron absorber. The hadron absorber was installed because the beam intensity is high and results in many main strong interactions in the target. For this reason the first tracking detectors upstream of SM1 have occupancies which are too high for tracking. Therefore the hadron absorber was installed to prevent all particles except muons from entering the spectrometer.

The hadron absorber was placed just downstream of the two target cells as can be seen in Fig. 1.23. The absorber corresponded to approximately 7.5 interactions lengths of material where the material was mostly alumina ( $\text{Al}_2\text{O}_3$ ) and concrete. Inside the absorber was an aluminum target followed by a tungsten plug, each of radius 2.5 cm. The tungsten was used as a beam dump while the aluminum was present to prevent back scattering from the tungsten beam plug. A side view showing the dimensions and materials used can be seen in Fig. 1.24. Both the aluminum target and tungsten plug served the double purposes as absorbers and also as unpolarized nuclear targets. In addition to the hadron absorber two thin  ${}^6\text{Li}$  absorbers were added just downstream of the primary absorber to absorb thermal neutrons produced in the primary absorber. This  ${}^6\text{Li}$  absorber was proposed to improve the performance of the first tracking detector downstream of the target even with the hadron absorber installed.

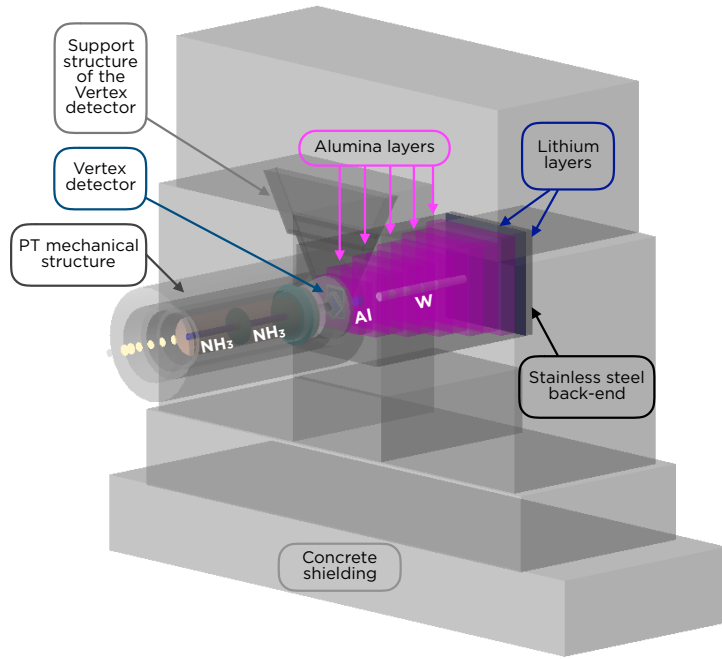


Figure 1.23: The hadron absorber downstream of the polarized target in 2015

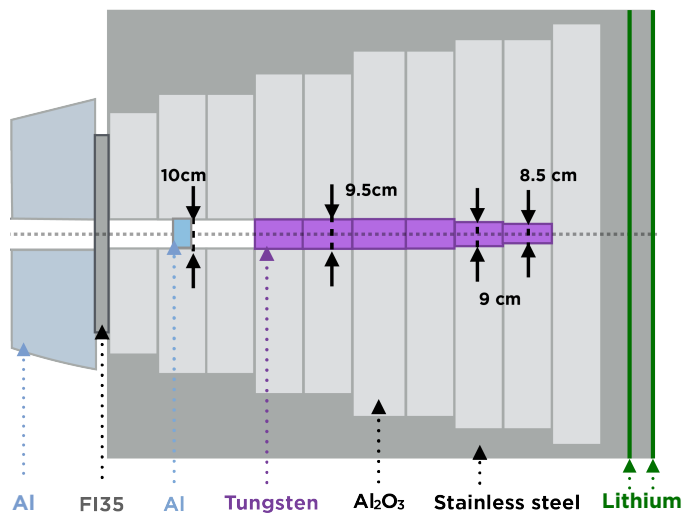


Figure 1.24: Side view of the hadron absorber used in 2015

# References

- [1] P. Abbon et al. The COMPASS experiment at CERN. *Nucl. Instrum. Meth.*, A577:455–518, 2007.
- [2] A. Abragam and M. Goldman. Principles of dynamic nuclear polarisation. *Reports on Progress in Physics*, 41:395–467, 1978.
- [3] V. Yu. Aleksakhin, Y. Bedfer, S. Gerasimov, and A. Yu. Korzenev. Geometrical event reconstruction in the COMPASS experiment. *Phys. Part. Nucl. Lett.*, 4:350–362, 2007. [Pisma Fiz. Elem. Chast. Atom. Yadra2007,no.4,588(2007)].
- [4] Radja Boughezal, John M. Campbell, R. Keith Ellis, Christfried Focke, Walter Giele, Xiaohui Liu, Frank Petriello, and Ciaran Williams. Color singlet production at NNLO in MCFM. *Eur. Phys. J.*, C77(1):7, 2017.
- [5] R. Fruhwirth. Application of Kalman filtering to track and vertex fitting. *Nucl. Instrum. Meth.*, A262:444–450, 1987.
- [6] Torbjrn Sjstrand, Stefan Ask, Jesper R. Christiansen, Richard Corke, Nishita Desai, Philip Ilten, Stephen Mrenna, Stefan Prestel, Christine O. Rasmussen, and Peter Z. Skands. An Introduction to PYTHIA 8.2. *Comput. Phys. Commun.*, 191:159–177, 2015.